ACS OMEGA

http://pubs.acs.org/journal/acsodf

Article

Study of the Hydrogen Storage Properties and Catalytic Mechanism of a MgH_2–Na_3AlH_6 System Incorporating $FeCl_3$

Muhammad Firdaus Asyraf Abdul Halim Yap, Muhammad Syarifuddin Yahya, Noratiqah Sazelee, Nurul Amirah Ali, Nurul Shafikah Mustafa, Nurul Nafiqah Sulaiman, and Mohammad Ismail*

Cite This: *ACS Omega* 2021, 6, 18948–18956

Read Online

ACCESS | Metrics & More | Article Recommendations | Supporting Information

ABSTRACT: In this work, the catalytic effects of $FeCl_3$ toward the hydrogen storage properties of the MgH_2–Na_3AlH_6 composite were investigated for the first time. The temperature-programed desorption results indicated that the onset temperature of the hydrogen release of a 10 wt % $FeCl_3$-doped MgH_2–Na_3AlH_6 composite was ~30 °C lower than that of the undoped MgH_2–Na_3AlH_6 composite. The addition of $FeCl_3$ into the MgH_2–Na_3AlH_6 composite resulted in improved absorption and desorption kinetics performance. The absorption/desorption kinetics measurements at 320 °C (under 33 and 1 atm hydrogen pressure, respectively) indicated that within 10 min, the doped sample absorbed ~4.0 wt % and desorbed ~1.5 wt % hydrogen. By comparison, the undoped sample absorbed only ~2.1 wt % and desorbed only ~0.6 wt % hydrogen under the same conditions and time. Comparably, the apparent activation energy value of the doped composite is 128 kJ/mol, which is 12 kJ/mol lower than that of the undoped composite (140 kJ/mol). The formation of the new species of $MgCl_2$ and Fe in the doped composite was detected from X-ray diffraction analysis after heating and absorption processes. These two components were believed to play a vital role in reducing the decomposition temperature and kinetics enhancement of the MgH_2–Na_3AlH_6 composite.

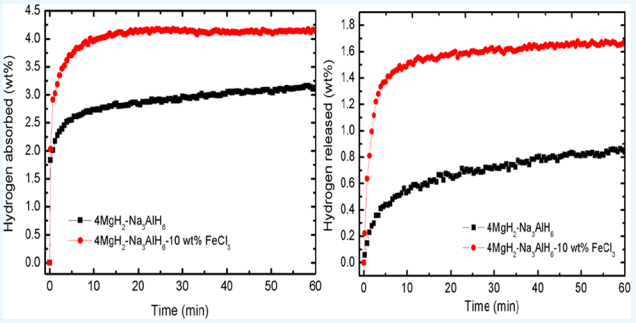

INTRODUCTION

The development of efficient and safe hydrogen storage technology is required to commercialize the hydrogen economy. So far, several states of storing hydrogen have been explored, namely, gaseous state,[1−3] liquid state,[4−6] and solid state.[7−14] Each of these kinds of storage has its own benefits. However, storing hydrogen in the solid state has more benefits, particularly regarding its safety and high volumetric hydrogen capacity. In recent years, a Mg-based hydride material, MgH_2, has been promptly promoted in numerous studies because of its high hydrogen release (7.6 wt %), good reversibility,[15−18] and highest energy density (9 MJ/kg).[19] Besides, $NaAlH_4$ is also a potential candidate to store hydrogen in the solid state due to its high theoretical hydrogen capacity (7.4 wt %).[20] However, the high temperature of hydrogen release (up to 400 °C for MgH_2 and up to 200 °C for $NaAlH_4$)[21−23] and poor sorption kinetics have impeded the practical use of MgH_2 and $NaAlH_4$ as the hydrogen storage medium.[24−26] To deal with these issues, a number of methods like enhancing the kinetics performance and lowering the decomposition temperature by doping with a potential catalyst[27−40] and improving the surface properties using the ball milling method[41,42] have been widely studied by many researchers.

Apart from the stated methods, reacting with other hydrides is one of the alternative methods that have been applied in solid-state hydrogen storage research to obtain better hydrogen storage performance. In recent years, this type of method has grown rapidly in finding potential solid-state hydrogen storage materials.[43−48] Previous research indicated that decomposition temperatures of as-milled MgH_2 and as-milled Na_3AlH_6 were reduced to approximately 55 °C after the reaction of MgH_2 and Na_3AlH_6.[49]

By the combination of the two hydrides, the enthalpy reaction can be improved, but it still cannot meet the practical application of hydrogen storage as a suitable requirement. Thus, a catalyst is used to enhance the sorption properties of the destabilized MgH_2–Na_3AlH_6 system. Our previous study demonstrated that the catalyst based on the metal fluorides had significantly improved hydrogen storage properties of the MgH_2–Na_3AlH_6 system.[50] The TiF_3-doped MgH_2–Na_3AlH_6 sample began releasing hydrogen at 140 °C, which is 30 °C

Received: April 27, 2021
Accepted: July 6, 2021
Published: July 15, 2021

lower than the undoped $MgH_2-Na_3AlH_6$. The reaction mechanism analysis indicated that the formation of NaF, AlF_3, and Al_3Ti plays a dominant role by serving as an active mechanism for nucleation and growth of dehydrogenated products.

Motivated by our previous research, another catalyst from a different metal group, namely, iron chloride ($FeCl_3$), was introduced to study its effect on the $MgH_2-Na_3AlH_6$ composite. To the best of our knowledge, no report has been claimed on the application of $FeCl_3$ as the catalyst for the hydrogen storage properties of the $MgH_2-Na_3AlH_6$ system to date. The effect of $FeCl_3$ on the Li−N−H system reported by Zhang et al.[51] demonstrated that the dehydrogenation peak and termination temperature of the doped 1 mol % $FeCl_3$ sample had been reduced, and the apparent activation energy was reduced by approximately 14.93 kJ/mol. Hence, it is interesting for this research to explore the effect of $FeCl_3$ on the hydrogen storage properties of the $MgH_2-Na_3AlH_6$ composite and gain an understanding of the nature and catalytic mechanism of the catalyst in the system. Hydrogenation properties and thermal properties were studied by pressure composition temperature (PCT) and differential scanning calorimetry (DSC), respectively. Meanwhile, the surface morphology of the sample was determined by scanning electron microscopy (SEM), and the structural characterization of the samples was determined by X-ray diffraction (XRD).

RESULTS AND DISCUSSION

Characterization of Na_3AlH_6. The XRD characterization of the NaH−$NaAlH_4$ (2:1) composite after milling for 20 h is displayed in Figure 1. The XRD pattern indicates that only

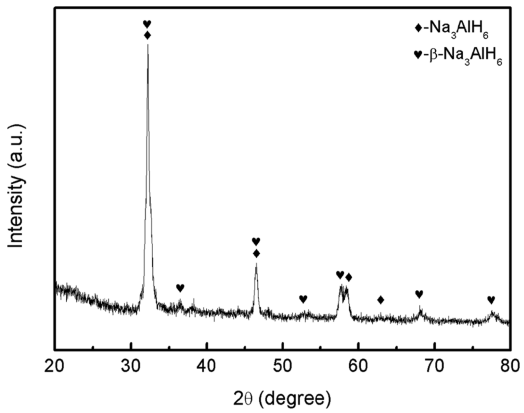

Figure 1. XRD profile of the NaH−$NaAlH_4$ (2:1) composite milled for 20 h.

Na_3AlH_6 peaks were present, whereas the peaks of NaH and $NaAlH_4$ were absent, indicating a complete transformation, which is represented by eq 1

$$2NaH + NaAlH_4 \rightarrow Na_3AlH_6 \quad (1)$$

The metastable β-Na_3AlH_6 peaks were also detected after the process of ball milling. It is expected that the polymorphic transformation of Na_3AlH_6 and β-Na_3AlH_6 has partially occurred as reported in previous work.[52]

Dehydrogenation Temperature. Figure 2 illustrates the TPD performance of the as-milled MgH_2, as-milled Na_3AlH_6, $MgH_2-Na_3AlH_6$ composite, and $MgH_2-Na_3AlH_6$−10 wt % $FeCl_3$. As displayed in Figure 2, the as-milled MgH_2 and Na_3AlH_6 exhibit the same decomposition process, which is only one dehydrogenation step. The dehydrogenation process of each one of the samples starts at around 350 and 230 °C. By comparing the decomposition properties, the $MgH_2-Na_3AlH_6$ composite with and without a catalyst has three dehydrogenation steps. These properties could have corresponded to the decomposition of Na_3AlH_6 and MgH_2 during the heating process. For the composite without a catalyst, the first dehydrogenation process had started at 170 °C and released 1.0 wt % hydrogen after heating at 220 °C. Next, the dehydrogenation process in the second stage occurred within 270−350 °C. Then, the third dehydrogenation process with a total hydrogen release of 5.9 wt % occurred at 375 °C. Meanwhile, the onset temperature for the composite with $FeCl_3$ is 140 °C, which results in the reduction of the decomposition temperature compared to the pristine $MgH_2-Na_3AlH_6$ composite. With further heating, the dehydrogenation process for the second stage takes place at 270−350 °C, and the third stage occurs at 360−450 °C.

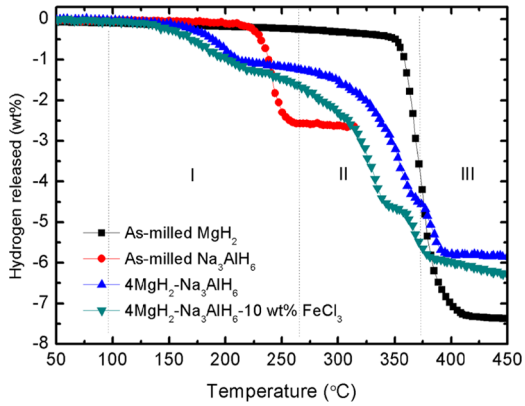

Figure 2. TPD profile of the as-milled MgH_2, as-milled Na_3AlH_6, $MgH_2-Na_3AlH_6$, and $MgH_2-Na_3AlH_6$−10 wt % $FeCl_3$ composites.

Sorption Kinetics Properties. The rehydrogenation of the dehydrogenated samples of $MgH_2-Na_3AlH_6$ with a 10 wt % $FeCl_3$ catalyst was conducted for the reversibility property. Figure 3 displays the rehydrogenation kinetics profile of the studied materials at 33 atm hydrogen pressure and an operating temperature of 320 °C. For a duration of 60 min, approximately 4.2 wt % hydrogen was absorbed by the catalyzed composite, whereas it was approximately 3.1 wt % for

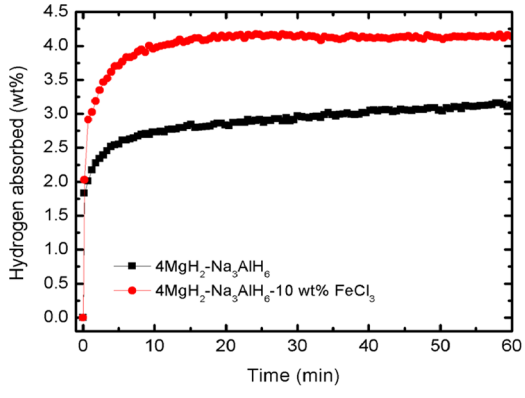

Figure 3. Rehydrogenation kinetics under a constant temperature of the composites at 320 °C and under 33 atm.

https://doi.org/10.1021/acsomega.1c02208
ACS Omega 2021, 6, 18948−18956

the pristine composite under a similar test condition. These results indicate that the absorption properties and the rehydrogenation process of the $MgH_2-Na_3AlH_6$ system were enhanced by the addition of $FeCl_3$.

The catalytic effect of $FeCl_3$ on the dehydrogenation properties of materials was explored at 1 atm in 60 min and an operating temperature of 320 °C, as illustrated in Figure 4.

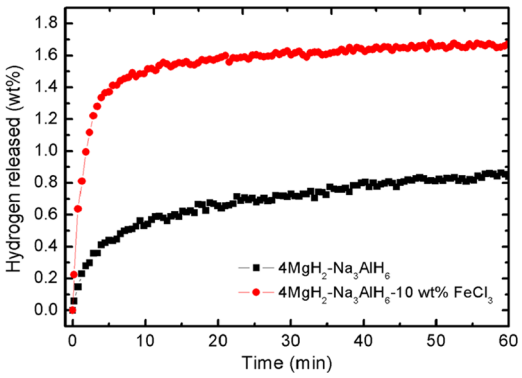

Figure 4. Dehydrogenation kinetics under a constant temperature of the materials at 320 °C and 1 atm hydrogen pressure.

For comparison, the undoped composite was characterized under the same condition. It can be observed that in 60 min, the catalyzed composite released approximately 1.7 wt % hydrogen at 320 °C. Conversely, the composite without the catalyst released 0.85 wt % hydrogen. These results indicate that the addition of $FeCl_3$ contributed to improving the desorption kinetics. The comparison of the hydrogen storage properties of $4MgH_2-Na_3AlH_6$ doped with different catalysts is shown in Table 1. Clearly, the onset dehydrogenation temperature of the $FeCl_3$-doped $MgH_2-Na_3AlH_4$ sample is lower than that of the $SrTiO_3$-doped $MgH_2-Na_3AlH_4$ sample. For the rehydrogenation kinetic performance, the $FeCl_3$-doped $MgH_2-Na_3AlH_4$ sample is better than the TiF_3- and $SrTiO_3$-doped $MgH_2-Na_3AlH_4$ samples. In addition, compared with other Mg–Al–H systems, such as $Mg(AlH_4)_2$ that was synthesized by high-energy ball milling of $Mg(AlH_4)_2(Et_2O)$ in a specially designed jar,[53] the $MgH_2-Na_3AlH_4$ system showed a slightly higher onset decomposition temperature. According to Pang et al.,[53] the as-synthesized $Mg(AlH_4)_2$ nanorods start to decompose at about 130 °C and 9.0 wt % hydrogen capacity was released within a two-step reaction.

Kinetic models can be used to further analyze the behavior of the sorption kinetics of the composite. In this study, the absorption and desorption behavior of the composites have been calculated using two kinetics models: (i) contracting volume and (ii) Johnson–Mehl–Avrami (JMA). The models are considered because the experimental data can be fitted to the models, and they are relatively accurate, as mentioned by Pang and Li.[55] The experimental data and the kinetics equation can be used to deduce the rate-limiting step of the kinetics process. The best linear plot from the models represents the rate-limiting step of the sorption behavior.

The calculation of the kinetic models based on equations in Table S1 (Supporting Information) is performed for the sorption kinetics operated at 320 °C and is illustrated in Figure 5. The calculations for both cases were done for a hydrogen

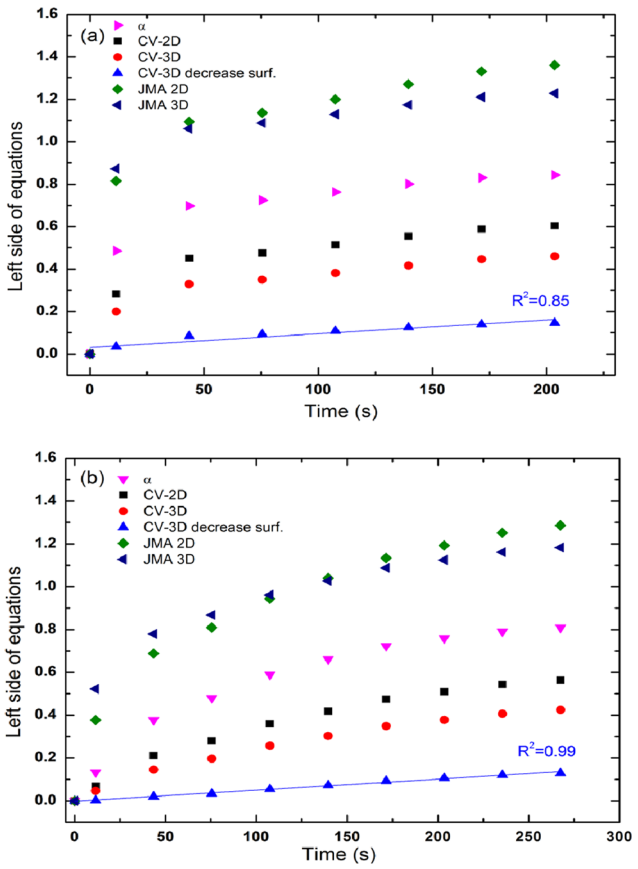

Figure 5. Calculation result of different kinetics equations of the $MgH_2-Na_3AlH_6$–10 wt % $FeCl_3$ composite based on Table 1 for (a) absorption at 320 °C and (b) desorption at 320 °C.

capacity range of 0–80%.[56] The result indicates that the rate-limiting step of the absorption and desorption of the doped composite at 320 °C is the diffusion of 3D growth that is regulated by reducing the interface velocity.

Thermal Properties. DSC curves of the doped and undoped $MgH_2-Na_3AlH_6$ composites at 20 °C/min (heating rate) are plotted in Figure 6. Two endothermic peaks of the undoped composite were observed at temperatures of 250 °C (first peak) and 390 °C (second peak). These endothermic peaks were attributed to the decomposition process of Na_3AlH_6[57] and MgH_2,[25] respectively. For the doped composite, two decomposition peaks were observed in which the peaks were decomposed at a lower temperature as compared to that for the undoped composite. The first and

Table 1. Comparison of the Hydrogen Storage Properties of $4MgH_2-Na_3AlH_6$ Doped with Different Catalysts

system	dehydrogenation temperature (°C)	rehydrogenation time (min)	hydrogen absorb (wt %)
$4MgH_2-Na_3AlH_6$ + TiF_3[50]	140.0	10.0	3.3
$4MgH_2-Na_3AlH_6$ + $SrTiO_3$[54]	145.0	10.0	3.7
$4MgH_2-Na_3AlH_6$ + $FeCl_3$ (this work)	140.0	10.0	4.0

https://doi.org/10.1021/acsomega.1c02208
ACS Omega 2021, 6, 18948–18956

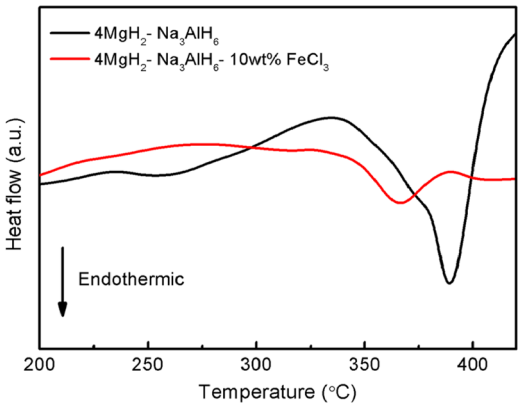

Figure 6. DSC profiles at 20 °C/min for the MgH_2−Na_3AlH_6 and MgH_2−Na_3AlH_6−10 wt % $FeCl_3$ samples.

second peaks were decomposed at 240 and 365 °C, respectively. There is a reduction of around 10 and 25 °C in the decomposition temperature compared to that of the undoped composite. These findings are compatible with the TPD outcomes described in Figure 2 but at a higher temperature. The disparity in the measurement condition between the two methods might be the reason for this phenomenon, as discussed in previous studies.[58,59]

Apparent Activation Energy. To determine the effect of the introduction of $FeCl_3$ on the kinetic characteristic of the MgH_2−Na_3AlH_6 composite system, the apparent activation energy for hydrogen release from the MgH_2−Na_3AlH_6−10 wt % $FeCl_3$ sample was investigated. The apparent activation energy of the undoped composite was also measured for comparison. A Kissinger plot was developed based on the Kissinger equation[60] presented as follows to determine the value of activation energy

$$\ln[\beta/T_P^2] = -E_A/RT_P + A \quad (2)$$

where β is the heating rate, T_P is the temperature of the peak in the DSC curve, R is given as the gas constant, and A is the linear constant. Meanwhile, in a graph of $\ln[\beta/T_P^2]$ against $1000/T_P$, the apparent activation energy, E_A, can be calculated from the slope. Figure 7a,b indicates the DSC curves for the undoped and doped samples at different heating rates.

The apparent activation energy for the decomposition of MgH_2 (second stage) of the undoped composite is 140 kJ/mol, based on the Kissinger analysis illustrated in Figure 8. By contrast, the apparent activation energy for the decomposition

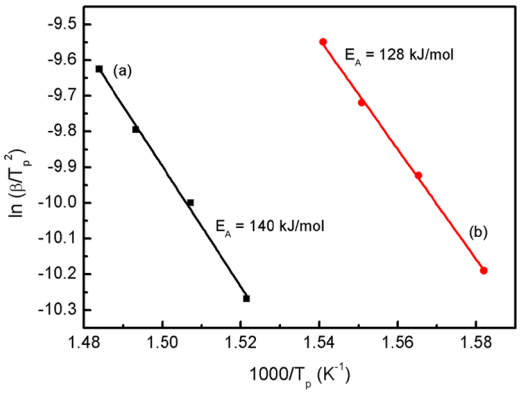

Figure 8. Kissinger analysis of (a) the MgH_2−Na_3AlH_6 and (b) MgH_2−Na_3AlH_6−10 wt % $FeCl_3$ composites.

of MgH_2 (second stage) of the doped composite was calculated to be 128 kJ/mol. The value for the reduction is approximately 12 kJ/mol. These values indicate that the $FeCl_3$ additive played a crucial role in decreasing the activation energy of the $4MgH_2$−Na_3AlH_6 composite.

Scanning Electron Microscopy Analysis. Figure 9 illustrates the morphologies of the doped and undoped MgH_2−Na_3AlH_6 composites with $FeCl_3$. Morphologies of pure MgH_2, milled MgH_2, milled Na_3AlH_6, and pure $FeCl_3$ have been added for comparison purposes. The pure particle image of MgH_2 reveals an angular thin shape that is larger than 50 μm (Figure 9a). After milling for 1 h, particle sizes were reduced and less homogeneous for MgH_2, as illustrated in Figure 9b. Figure 9c presents the SEM image of milled Na_3AlH_6 in which the particle is deposited in a coral-like shape. Meanwhile, the SEM image of the as-received $FeCl_3$ is presented in Figure 9d. The particles' sizes are larger than 1 μm without any further purification. Additionally, the MgH_2−Na_3AlH_6 composite shows a decrease in particle sizes, as illustrated in Figure 9e. Following the addition of $FeCl_3$ to the composite MgH_2−Na_3AlH_6 (Figure 9f), the particle sizes were decreased relative to the undoped composite. Smaller particle sizes can improve the absorption performance of the hydrogen because they increase the total particle reaction surface area and minimize the hydrogen diffusion length.[61]

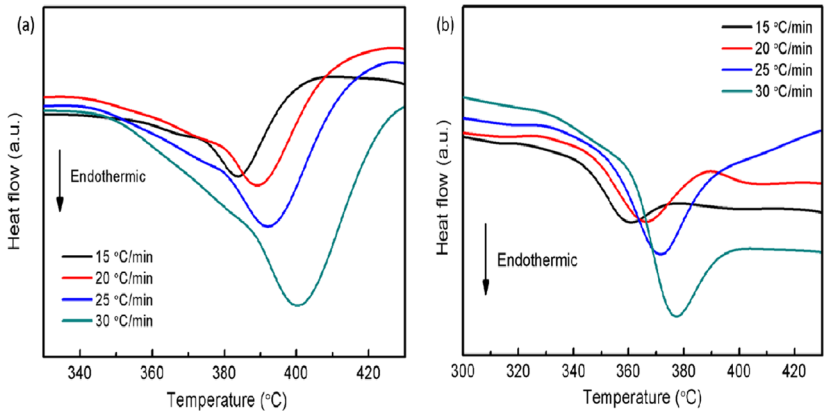

Figure 7. DSC curves of (a) the MgH_2−Na_3AlH_6 composite and (b) the MgH_2−Na_3AlH_6−10 wt % $FeCl_3$ composite at different heating ramps (15, 20, 25, and 30 °C/min).

https://doi.org/10.1021/acsomega.1c02208
ACS Omega 2021, 6, 18948−18956

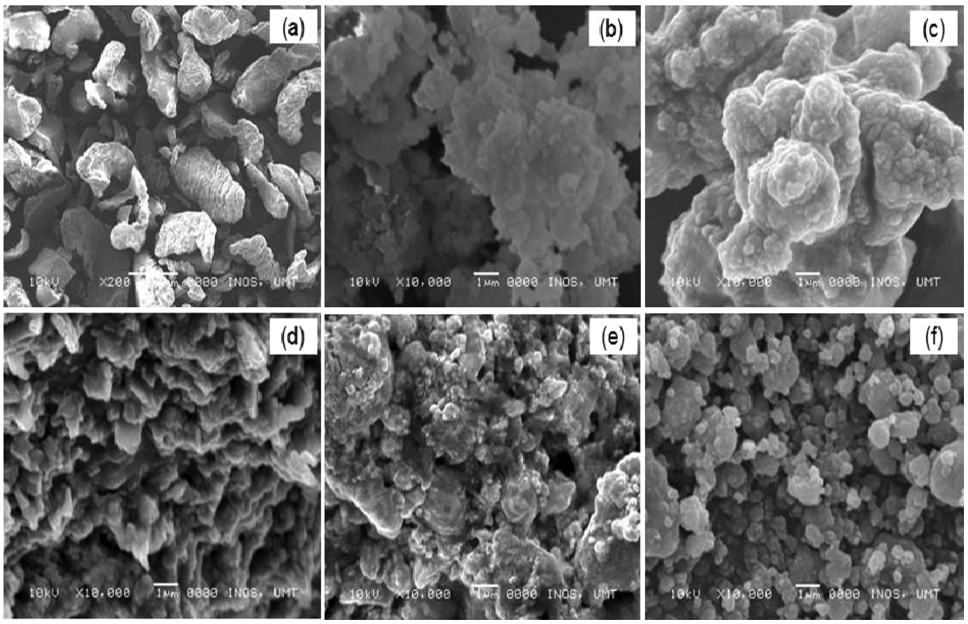

Figure 9. Surface morphology of pure MgH_2 (a), milled MgH_2 (b), milled Na_3AlH_6 (c), pure $FeCl_3$ (d), MgH_2−Na_3AlH_6 composite (e), and MgH_2−Na_3AlH_6−10 wt % $FeCl_3$ composite (f).

Reaction Mechanism Analysis. The XRD analysis results at various stages of dehydrogenation for the undoped MgH_2−Na_3AlH_6 composite are illustrated in Figure 10. After a 60 min process of ball milling, peaks of MgH_2, Na_3AlH_6, and metastable β-Na_3AlH_6 appeared (Figure 10a). New hydride phases in the form of perovskite, $NaMgH_3$ and MgH_2, that did not react were observed at the first stage of the 230 °C dehydrogenation process (Figure 10b). This phenomenon occurred because the Na_3AlH_6 phase disappeared after the process of heating. Moreover, there were a few Al peaks that were clearly observed after the desorption process at 230 °C. The formation of $NaMgH_3$ and Al peaks was due to the decomposition of Na_3AlH_6 that had reacted with MgH_2, as displayed in eq 3

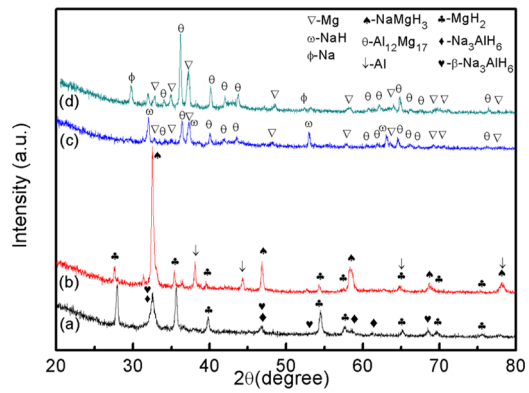

Figure 10. XRD profiles of the MgH_2−Na_3AlH_6 sample (a) after 1 h of milling and after desorption at (b) 230 °C, (c) 375 °C, and (d) 450 °C.

$$Na_3AlH_6 + 3MgH_2 \rightarrow 3NaMgH_3 + Al + 3/2H_2 \quad (3)$$

In Figure 10c, when the MgH_2−Na_3AlH_6 composite was heated to 375 °C, the NaH phase was detected. However, the intermediate peaks of $Mg_{17}Al_{12}$ and Mg dominated the XRD phase. Furthermore, phases of MgH_2 and $NaMgH_3$ disappeared. The observation of the diffraction peaks indicated that the desorption of hydrogen at 375 °C corresponded to MgH_2 whose decomposition and reaction with Al are presented in eqs 4 and 5, respectively. Meanwhile, the decomposition of $NaMgH_3$ is represented by eq 6.

$$MgH_2 \rightarrow Mg + H_2 \quad (4)$$

$$17MgH_2 + 12Al \rightarrow Mg_{17}Al_{12} + 17H_2 \quad (5)$$

$$NaMgH_3 \rightarrow NaH + Mg + H_2 \quad (6)$$

When the process temperature was increased up to 450 °C, as displayed in Figure 10d, the peak of Na was detected. It was believed that the NaH phase had fully dehydrogenated at this stage, as illustrated in eq 7

$$NaH \rightarrow Na + 1/2H_2 \quad (7)$$

To clarify the impact of $FeCl_3$ on the destabilized MgH_2−Na_3AlH_6 system, the XRD measurements were also conducted at various dehydrogenation stages, as illustrated in Figure 11. The peaks of MgH_2, Na_3AlH_6, metastable β-Na_3AlH_6, and $FeCl_3$ were detected after 60 min of ball milling, as illustrated in Figure 11a. When the $FeCl_3$-doped MgH_2−Na_3AlH_6 sample was heated at 220 °C, new phases, Fe and $MgCl_2$, were detected from the XRD pattern (Figure 11b). Additionally, MgH_2, $NaMgH_3$, and Al species also appeared, which are liable for improving the desorption temperature of the MgH_2−Na_3AlH_6 system. Additional phases were detected after the heating process at 350 and 420 °C and are depicted in Figure 11c,d, respectively. These results indicate that new species of $MgCl_2$ and Fe that formed and acted as the active species were due to the reaction between $FeCl_3$ and Mg components, as illustrated in eq 8

$$3MgH_2 + 2FeCl_3 \rightarrow 3MgCl_2 + 2Fe + 3H_2 \quad (8)$$

The XRD analysis was run for $4MgH_2$−Na_3AlH_6 and the destabilized MgH_2−Na_3AlH_6−10 wt % $FeCl_3$ system to

https://doi.org/10.1021/acsomega.1c02208
ACS Omega 2021, 6, 18948−18956

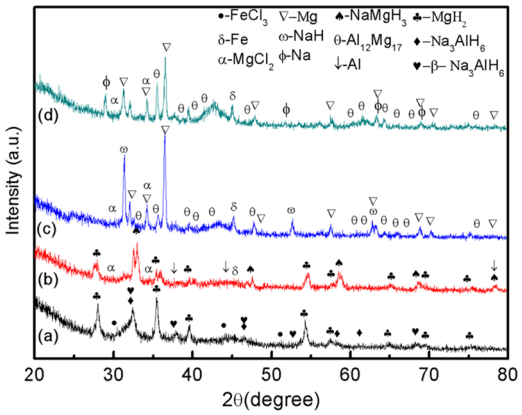

Figure 11. XRD profiles of the MgH_2−Na_3AlH_6−10 wt % $FeCl_3$ sample (a) after 1 h of milling and after desorption at (b) 220 °C, (c) 350 °C, and (d) 420 °C.

examine the reaction mechanism after the absorption process. These measurements were carried out under 33 atm H_2 pressure at 320 °C, as depicted in Figure 12. Figure 12a

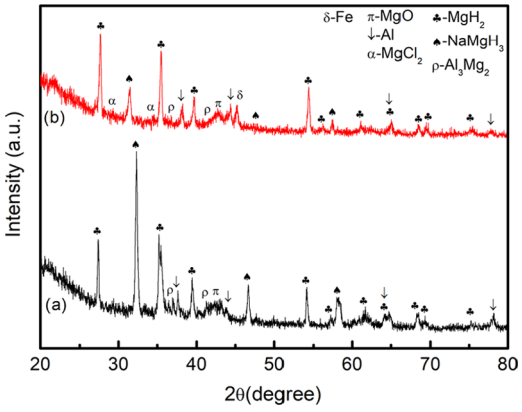

Figure 12. XRD profiles of the (a) MgH_2−Na_3AlH_6 and (b) the MgH_2−Na_3AlH_6−10 wt % $FeCl_3$ composites after absorption at 320 °C.

indicates that $NaMgH_3$, Al_3Mg_2, MgH_2, Al, and MgO phases can be identified in the MgH_2−Na_3AlH_6 sample. After addition of $FeCl_3$ (Figure 12b), Fe and $MgCl_2$ were detected in the doped composite. The diffraction peaks were previously observed in the destabilized MgH_2−Na_3AlH_6−10 wt % $FeCl_3$ system after dehydrogenation. The peaks of $Mg_{17}Al_{12}$ and Mg disappeared after the absorption process for undoped and doped samples. These results indicated full conversion of MgH_2, as illustrated in eq 9

$$Mg_{17}Al_{12} + (17 - 2y)H_2 \rightarrow yMg_2Al_3 + (17 - 2y)MgH_2 + (12 - 3y)Al \quad (9)$$

The formation of Fe and $MgCl_2$ species during the desorption process with the addition of $FeCl_3$ could play a significant role in enhancing the hydrogen sorption performances of the MgH_2−Na_3AlH_6 composite. Fe is well known for being a promising catalyst for MgH_2.[62−64] The in situ formed Fe may interact with molecules of hydrogen and cause hydrogen molecules to dissociate, subsequently boosting the re/dehydrogenation kinetics. Meanwhile, the catalytic effect of Cl-containing species ($MgCl_2$) may also have an impact on the sorption kinetics. $MgCl_2$ plays a crucial part in ameliorating the rehydrogenation kinetics of MgH_2 doped with $NiCl_2$ and $CoCl_2$, as reported by Mao et al.[65] Additionally, the desorption and absorption kinetics can be enhanced by shortening the diffusion distance of reaction ions from $MgCl_2$ and like an active site for the products of the nucleation and desorption. Thus, the newly developed products, $MgCl_2$ and Fe, have a promising catalytic impact on enhancing the hydrogen sorption performances of the destabilized MgH_2−Na_3AlH_6 system. Therefore, these new species also served as active sites for the dehydrogenated products in nucleation and growth, thus enhancing the hydrogen sorption properties of the MgH_2−Na_3AlH_6 system.

CONCLUSIONS

In summary, doping with the $FeCl_3$ catalyst increased the efficiency of the MgH_2−Na_3AlH_6 composite in hydrogen storage. The $FeCl_3$-doped MgH_2−Na_3AlH_6 composite starts to release hydrogen at approximately 140 °C, which is approximately 30 °C lower than the onset dehydrogenation temperature of the undoped $4MgH_2$−Na_3AlH_6 composite. Additionally, the absorption and desorption kinetics of the MgH_2−Na_3AlH_6 composite were reinforced by the addition of $FeCl_3$. The apparent activation energy for MgH_2-relevant decomposition in the MgH_2−Na_3AlH_6 composite was decreased from 140 to 128 kJ/mol utilizing $FeCl_3$ from the Kissinger plot. For the SEM images, the doped composite displayed smaller sizes of particles compared to those of the undoped composite. These improvements were made possible by the formation of catalytic species, Fe and $MgCl_2$, during the heating processes. It is rational to assume that the development of such active species increased the interaction between MgH_2 and Na_3AlH_6, thus further enhancing the efficiency of the MgH_2−Na_3AlH_6 system in hydrogen storage.

EXPERIMENTAL DETAILS

Starting materials, magnesium hydride (MgH_2), sodium hydride (NaH), sodium aluminum hydride ($NaAlH_4$), and iron(III) chloride ($FeCl_3$) were purchased from Sigma-Aldrich with nearly 100% purity. Na_3AlH_6 was synthesized through the mechanochemical reaction by mixing NaH and $NaAlH_4$ at a molar ratio of 2:1.[66] The composite made of MgH_2 and Na_3AlH_6 with a mole ratio of 4:1 (denoted as MgH_2−Na_3AlH_6) and the $FeCl_3$ catalyst were milled in a planetary ball mill (NQM-04) for 1 h at a rotation speed of 400 rpm. The sample was placed into a sealed stainless steel vial together with hardened stainless steel balls. The ball-to-powder ratio in terms of weight was 40:1. To avoid the exposure of samples to moisture, all sample preparations were conducted in a glovebox (MBraun Unilab) under an inert gas atmosphere (argon).

For the temperature-programed desorption (TPD) measurement, a sample of approximately 60 mg was heated from room temperature to 450 °C at a 5 °C/min heating rate in a Sieverts-type PCT apparatus. Moreover, the absorption and desorption kinetics were investigated at a constant temperature of 320 °C under 33 and 1 atm hydrogen pressure, respectively. For the evaluation of the thermal properties of samples, the DSC measurement was conducted using a Mettler Toledo TGA/DCS 1. Around 5 mg of samples were heated from room temperature to 450 °C under an argon flow and different heating rates (15, 20, 25, and 30 °C/min) were used.

https://doi.org/10.1021/acsomega.1c02208
ACS Omega 2021, 6, 18948−18956

A scanning electron microscope (JEOLJSM-6360LA) was used to determine the morphology of the as-received MgH_2, as-milled MgH_2, synthesized Na_3AlH_6, and as-milled MgH_2−Na_3AlH_6 composite with and without $FeCl_3$. Meanwhile, reaction mechanisms of the $FeCl_3$-doped MgH_2−Na_3AlH_6 composite after the milling and decomposition and after the absorption processes were evaluated by an X-ray diffractometer (Rigaku MiniFlex). The scans were carried out over diffraction angles from 20 to 80° at a speed of 2.00°/min.

■ ASSOCIATED CONTENT

Supporting Information

The Supporting Information is available free of charge at https://pubs.acs.org/doi/10.1021/acsomega.1c02208.

Additional information for the calculation of sorption kinetic models (PDF)

■ AUTHOR INFORMATION

Corresponding Author

Mohammad Ismail − *Energy Storage Research Group, Faculty of Ocean Engineering Technology and Informatics, Universiti Malaysia Terengganu, 21030 Kuala Nerus, Malaysia;* orcid.org/0000-0002-1946-9007; Phone: +609-6683487; Email: mohammadismail@umt.edu.my; Fax: +609-6683991

Authors

Muhammad Firdaus Asyraf Abdul Halim Yap − *Energy Storage Research Group, Faculty of Ocean Engineering Technology and Informatics, Universiti Malaysia Terengganu, 21030 Kuala Nerus, Malaysia; Faculty of Innovative Design and Technology, Universiti Sultan Zainal Abidin, 21300 Kuala Nerus, Terengganu, Malaysia*

Muhammad Syarifuddin Yahya − *Energy Storage Research Group, Faculty of Ocean Engineering Technology and Informatics, Universiti Malaysia Terengganu, 21030 Kuala Nerus, Malaysia*

Noratiqah Sazelee − *Energy Storage Research Group, Faculty of Ocean Engineering Technology and Informatics, Universiti Malaysia Terengganu, 21030 Kuala Nerus, Malaysia*

Nurul Amirah Ali − *Energy Storage Research Group, Faculty of Ocean Engineering Technology and Informatics, Universiti Malaysia Terengganu, 21030 Kuala Nerus, Malaysia*

Nurul Shafikah Mustafa − *Energy Storage Research Group, Faculty of Ocean Engineering Technology and Informatics, Universiti Malaysia Terengganu, 21030 Kuala Nerus, Malaysia*

Nurul Nafiqah Sulaiman − *Energy Storage Research Group, Faculty of Ocean Engineering Technology and Informatics, Universiti Malaysia Terengganu, 21030 Kuala Nerus, Malaysia;* Present Address: Nuclear Technology Research Centre, Faculty of Science and Technology, Universiti Kebangsaan Malaysia, 43600 UKM Bangi, Selangor, Malaysia

Complete contact information is available at: https://pubs.acs.org/10.1021/acsomega.1c02208

Notes

The authors declare no competing financial interest.

■ ACKNOWLEDGMENTS

This work was funded by the Ministry of Higher Education Malaysia through the Fundamental Research Grant Scheme (FRGS, FRGS/1/2019/STG07/UMT/02/5). The authors also wish to express the deepest gratitude to Universiti Malaysia Terengganu for the facilities provided.

■ REFERENCES

(1) Zheng, J.; Liu, X.; Xu, P.; Liu, P.; Zhao, Y.; Yang, J. Development of high pressure gaseous hydrogen storage technologies. *Int. J. Hydrogen Energy* **2012**, *37*, 1048−1057.

(2) Walker, S. B.; Mukherjee, U.; Fowler, M.; Elkamel, A. Benchmarking and selection of power-to-gas utilizing electrolytic hydrogen as an energy storage alternative. *Int. J. Hydrogen Energy* **2016**, *41*, 7717−7731.

(3) Bailera, M.; Kezibri, N.; Romeo, L. M.; Espatolero, S.; Lisbona, P.; Bouallou, C. Future applications of hydrogen production and CO_2 utilization for energy storage: Hybrid power to gas-oxycombustion power plants. *Int. J. Hydrogen Energy* **2017**, *42*, 13625−13632.

(4) Peschka, W.; Carpetis, C. Cryogenic hydrogen storage and refueling for automobiles. *Int. J. Hydrogen Energy* **1980**, *5*, 619−625.

(5) Eypasch, M.; Schimpe, M.; Kanwar, A.; Hartmann, T.; Herzog, S.; Frank, T.; Hamacher, T. Model-based techno-economic evaluation of an electricity storage system based on Liquid Organic Hydrogen Carriers. *Appl. Energy* **2017**, *185*, 320−330.

(6) Liu, S.-Y.; Kundu, P.; Huang, T.-W.; Chuang, Y.-J.; Tseng, F.-G.; Lu, Y.; Sui, M.-L.; Chen, F.-R. Quasi-2D liquid cell for high density hydrogen storage. *Nano Energy* **2017**, *31*, 218−224.

(7) Cummings, D. L.; Powers, G. J. The storage of hydrogen as metal hydrides. *Ind. Eng. Chem. Process Des. Dev.* **1974**, *13*, 182−192.

(8) Rönnebro, E. Development of group II borohydrides as hydrogen storage materials. *Curr. Opin. Solid State Mater. Sci.* **2011**, *15*, 44−51.

(9) Lototskyy, M.; Yartys, V. A. Comparative analysis of the efficiencies of hydrogen storage systems utilising solid state H storage materials. *J. Alloys Compd.* **2015**, *645*, S365−S373.

(10) Niaz, S.; Manzoor, T.; Pandith, A. H. Hydrogen storage: Materials, methods and perspectives. *Renewable Sustainable Energy Rev.* **2015**, *50*, 457−469.

(11) Sazelee, N.; Mustafa, N. S.; Yahya, M. S.; Ismail, M. Enhanced dehydrogenation performance of $NaAlH_4$ by the addition of spherical $SrTiO_3$. *Int. J. Energy Res.* **2021**, 8648−8658.

(12) Yin, Y.; Qi, Y.; Li, B.; Gu, H.; Zhao, J.; Ji, L.; Zhang, B.; Yuan, Z.; Zhang, Y. A comparative study of NbF_5 catalytic effects on hydrogenation/dehydrogenation kinetics of Mg-Zn-Ni and Mg-Cu-Ni systems. *Mater. Charact.* **2021**, *174*, No. 110993.

(13) Yong, H.; Wei, X.; Hu, J.; Yuan, Z.; Wu, M.; Zhao, D.; Zhang, Y. Influence of Fe@C composite catalyst on the hydrogen storage properties of Mg−Ce−Y based alloy. *Renewable Energy* **2020**, *162*, 2153−2165.

(14) Mustafa, N. S.; Ismail, M. Enhanced hydrogen storage properties of $4MgH_2$ + $LiAlH_4$ composite system by doping with Fe_2O_3 nanopowder. *Int. J. Hydrogen Energy* **2014**, *39*, 7834−7841.

(15) Jain, I. P.; Lal, C.; Jain, A. Hydrogen storage in Mg: A most promising material. *Int. J. Hydrogen Energy* **2010**, *35*, 5133−5144.

(16) Grochala, W.; Edwards, P. P. Thermal decomposition of the non-interstitial hydrides for the storage and production of hydrogen. *Chem. Rev.* **2004**, *104*, 1283−1315.

(17) Milošević, S.; Milanovic, I.; Mamula, B. P.; Dukic, A.; Rajnovic, D.; Pasquini, L.; Novakovic, J. G. Hydrogen desorption properties of MgH_2 catalysed with $NaNH_2$. *Int. J. Hydrogen Energy* **2013**, *38*, 12223−12229.

(18) Huot, J.; Liang, G.; Boily, S.; Van Neste, A.; Schulz, R. Structural study and hydrogen sorption kinetics of ball-milled magnesium hydride. *J. Alloys Compd.* **1999**, *293*−*295*, 495−500.

(19) Sakintuna, B.; Lamari-Darkrim, F.; Hirscher, M. Metal hydride materials for solid hydrogen storage: A review. *Int. J. Hydrogen Energy* **2007**, *32*, 1121−1140.

(20) Zhao, L.; Xu, F.; Zhang, C.; Wang, Z.; Ju, H.; Gao, X.; Zhang, X.; Sun, L.; Liu, Z. Enhanced hydrogen storage of alanates: Recent progress and future perspectives. *Prog. Nat. Sci.: Mater. Int.* **2021**, *31*, 165−179.
(21) Wang, H.; Zhang, J.; Liu, J. W.; Ouyang, L. Z.; Zhu, M. Improving hydrogen storage properties of MgH_2 by addition of alkali hydroxides. *Int. J. Hydrogen Energy* **2013**, *38*, 10932−10938.
(22) Sazelee, N. A.; Idris, N. H.; Din, M. M.; Yahya, M. S.; Ali, N. A.; Ismail, M. $LaFeO_3$ synthesised by solid-state method for enhanced sorption properties of MgH_2. *Results Phys.* **2020**, *16*, No. 102844.
(23) Chen, W.; You, L.; Xia, G.; Yu, X. A balance between catalysis and nanoconfinement towards enhanced hydrogen storage performance of $NaAlH_4$. *J. Mater. Sci. Technol.* **2021**, *79*, 205−211.
(24) Hosseini, S. E.; Wahid, M. A. Hydrogen production from renewable and sustainable energy resources: Promising green energy carrier for clean development. *Renewable Sustainable Energy Rev.* **2016**, *57*, 850−866.
(25) Ding, Z.; Fu, Y.; Wang, Y.; Bi, J.; Zhang, L.; Peng, D.; Li, Y.; Han, S. $MgCNi_3$ prepared by powder metallurgy for improved hydrogen storage properties of MgH_2. *Int. J. Hydrogen Energy* **2019**, *44*, 8347−8356.
(26) Nersisyan, H. H.; Kim, W. B.; Choi, W. S.; Woo, H.-Y.; Hong, S.-J.; Lee, J. H. Rare-earth hexaboride 2D nanostructures synthesis and coupling with $NaAlH_4$ for improved hydrogen release. *Ceram. Int.* **2021**, *47*, 877−888.
(27) Kwak, Y. J.; Song, J.; Mumm, D. R. Improvement of hydrogen storage properties of Mg by addition of NbF_5 via mechanical milling under H_2. *Korean J. Mater. Res.* **2013**, *23*, 562−567.
(28) Youn, J.-S.; Phan, D.-T.; Park, C.-M.; Jeon, K.-J. Enhancement of hydrogen sorption properties of MgH_2 with a MgF_2 catalyst. *Int. J. Hydrogen Energy* **2017**, *42*, 20120−20124.
(29) Ismail, M. Effect of adding different percentages of $HfCl_4$ on the hydrogen storage properties of MgH_2. *Int. J. Hydrogen Energy* **2021**, *46*, 8621−8628.
(30) Kumar, S.; Jain, A.; Yamaguchi, S.; Miyaoka, H.; Ichikawa, T.; Mukherjee, A.; Dey, G.; Kojima, Y. Surface modification of MgH_2 by $ZrCl_4$ to tailor the reversible hydrogen storage performance. *Int. J. Hydrogen Energy* **2017**, *42*, 6152−6159.
(31) Sabitu, S. T.; Goudy, A. J. Dehydrogenation kinetics and modeling studies of MgH_2 Enhanced by transition metal oxide catalysts using constant pressure thermodynamic driving forces. *Metals* **2012**, *2*, 219−228.
(32) Meena, P.; Singh, R.; Sharma, V. K.; Jain, I. P. Role of $NiMn_{9.3}Al_{4.0}Co_{14.1}Fe_{3.6}$ alloy on dehydrogenation kinetics of MgH_2. *J. Magnesium Alloys* **2018**, *6*, 318−325.
(33) Yao, P.; Jiang, Y.; Liu, Y.; Wu, C.; Chou, K.-C.; Lyu, T.; Li, Q. Catalytic effect of Ni@rGO on the hydrogen storage properties of MgH_2. *J. Magnesium Alloys* **2020**, *8*, 461−471.
(34) Ismail, M.; Yahya, M. S.; Sazelee, N. A.; Ali, N. A.; Yap, F. A. H.; Mustafa, N. S. The effect of K_2SiF_6 on the MgH_2 hydrogen storage properties. *J. Magnesium Alloys* **2020**, *8*, 832−840.
(35) Pukazhselvan, D.; Nasani, N.; Yang, T.; Ramasamy, D.; Shaula, A.; Fagg, D. P. Chemically transformed additive phases in Mg_2TiO_4 and $MgTiO_3$ loaded hydrogen storage system MgH_2. *Appl. Surf. Sci.* **2019**, *472*, 99−104.
(36) Pukazhselvan, D.; Nasani, N.; Correia, P.; Carbó-Argibay, E.; Otero-Irurueta, G.; Stroppa, D. G.; Fagg, D. P. Evolution of reduced Ti containing phase(s) in MgH_2/TiO_2 system and its effect on the hydrogen storage behavior of MgH_2. *J. Power Sources* **2017**, *362*, 174−183.
(37) Li, Z.; Yu, J. Z.; Zhang, Y.; Liu, D. M.; Wang, C. Y.; Si, T. Z.; Li, Y. T.; Zhang, Q. A. Coupling of nanoconfinement with metallic catalysis in supported $NaAlH_4$ for low-temperature hydrogen storage. *J. Power Sources* **2021**, *491*, No. 229611.
(38) Ali, N. A.; Ismail, M. Modification of $NaAlH_4$ properties using catalysts for solid-state hydrogen storage: A review. *Int. J. Hydrogen Energy* **2021**, *46*, 766−782.
(39) Lu, X.; Zhang, L.; Yu, H.; Lu, Z.; He, J.; Zheng, J.; Wu, F.; Chen, L. Achieving superior hydrogen storage properties of MgH_2 by the effect of TiFe and carbon nanotubes. *Chem. Eng. J.* **2021**, *422*, No. 130101.
(40) Liu, H.; Lu, C.; Wang, X.; Xu, L.; Huang, X.; Wang, X.; Ning, H.; Lan, Z.; Guo, J. Combinations of V_2C and Ti_3C_2 MXenes for boosting the hydrogen storage performances of MgH_2. *ACS Appl. Mater. Interfaces* **2021**, *13*, 13235−13247.
(41) Huot, J.; Liang, G.; Boily, S.; Van Neste, A.; Schulz, R. Structural study and hydrogen sorption kinetics of ball-milled magnesium hydride. *J. Alloys Compd.* **1999**, *293*−*295*, 495−500.
(42) Han, Z.; Chen, H.; Li, X.; Jiang, R.; Zhou, S. Novel application of MgH_2/MoS_2 hydrogen storage materials to thiophene hydrodesulfurization: A combined experimental and theoretical case study. *Mater. Des.* **2018**, *158*, 213−223.
(43) Sulaiman, N. N.; Ismail, M.; Timmiati, S. N.; Lim, K. L. Improved hydrogen storage performances of $LiAlH_4$ + $Mg(BH_4)_2$ composite with TiF_3 addition. *Int. J. Energy Res.* **2021**, *45*, 2882−2898.
(44) Mao, J. F.; Yu, X. B.; Guo, Z. P.; Liu, H. K.; Wu, Z.; Ni, J. Enhanced hydrogen storage performances of $NaBH_4$-MgH_2 system. *J. Alloys Compd.* **2009**, *479*, 619−623.
(45) Ali, N. A.; Ismail, M. Advanced hydrogen storage of the Mg−Na−Al system: A review. *J. Magnesium Alloys* **2021**, *9*, 1111−1122.
(46) Liu, S.-S.; Sun, L.-X.; Zhang, J.; Zhang, Y.; Xu, F.; Xing, Y.-H.; Li, F.; Zhao, J.; Du, Y.; Hu, W.-Y.; Deng, H.-Q. Hydrogen storage properties of destabilized MgH_2−Li_3AlH_6 system. *Int. J. Hydrogen Energy* **2010**, *35*, 8122−8129.
(47) Sulaiman, N. N.; Ismail, M.; Rashid, A. H. A.; Ali, N. A.; Sazelee, N. A.; Timmiati, S. N. Hydrogen storage properties of Mg-Li-Al composite system doped with Al_2TiO_5 catalyst for solid-state hydrogen storage. *J. Alloys Compd.* **2021**, *870*, No. 159469.
(48) Gosalawit-Utke, R.; Milanese, C.; Nielsen, T. K.; Karimi, F.; Saldan, I.; Pranzas, K.; Jensen, T. R.; Marini, A.; Klassen, T.; Dornheim, M. Nanoconfined $2LiBH_4$-MgH_2 for reversible hydrogen storages: Reaction mechanisms, kinetics and thermodynamics. *Int. J. Hydrogen Energy* **2013**, *38*, 1932−1942.
(49) Ismail, M.; Zhao, Y.; Dou, S. X. An investigation on the hydrogen storage properties and reaction mechanism of the destabilized MgH_2−Na_3AlH_6 (4:1) system. *Int. J. Hydrogen Energy* **2013**, *38*, 1478−1483.
(50) Halim Yap, F. A.; Yahya, M. S.; Ismail, M. Enhancement of hydrogen storage properties in $4MgH_2$-Na_3AlH_6 composite catalyzed by TiF_3. *Int. J. Hydrogen Energy* **2017**, *42*, 21096−21104.
(51) Zhang, W.; Wang, H.; Cao, H.; He, T.; Guo, J.; Wu, G.; Chen, P. Effects of doping $FeCl_3$ on hydrogen storage properties of Li-N-H system. *Prog. Nat. Sci.: Mater. Int.* **2017**, *27*, 139−143.
(52) Wang, P.; Kang, X.; Cheng, H. Direct formation of Na_3AlH_6 by mechanical milling NaH/Al with TiF_3. *Appl. Phys. Lett.* **2005**, *87*, No. 071911.
(53) Pang, Y.; Liu, Y.; Gao, M.; Ouyang, L.; Liu, J.; Wang, H.; Zhu, M.; Pan, H. A mechanical-force-driven physical vapour deposition approach to fabricating complex hydride nanostructures. *Nat. Commun.* **2014**, *5*, No. 3519.
(54) Yahya, M. S.; Lew, W. B.; Halim Yap, F. A.; Ismail, M. The catalytic effect of an inert additive ($SrTiO_3$) on the hydrogen storage properties of $4MgH_2$-Na_3AlH_6. *Int. J. Hydrogen Energy* **2018**, *43*, 20801−20810.
(55) Pang, Y.; Li, Q. A review on kinetic models and corresponding analysis methods for hydrogen storage materials. *Int. J. Hydrogen Energy* **2016**, *41*, 18072−18087.
(56) Yonkeu, A. L.; Swainson, I. P.; Dufour, J.; Huot, J. Kinetic investigation of the catalytic effect of a body centered cubic-alloy $TiV_{1.1}Mn_{0.9}$ (BCC) on hydriding/dehydriding properties of magnesium. *J. Alloys Compd.* **2008**, *460*, 559−564.
(57) Wu, R.; Du, H.; Wang, Z.; Gao, M.; Pan, H.; Liu, Y. Remarkably improved hydrogen storage properties of $NaAlH_4$ doped with 2D titanium carbide. *J. Power Sources* **2016**, *327*, 519−525.
(58) Sazelee, N.; Yahya, M.; Idris, N.; Din, M. M.; Ismail, M. Desorption properties of $LiAlH_4$ doped with $LaFeO_3$ catalyst. *Int. J. Hydrogen Energy* **2019**, *44*, 11953−11960.

(59) Yahya, M. S.; Ismail, M. Improvement of hydrogen storage properties of MgH_2 catalyzed by K_2NbF_7 and multiwall carbon nanotube. *J. Phys. Chem. C* **2018**, *122*, 11222−11233.
(60) Kissinger, H. E. Reaction kinetics in differential thermal analysis. *Anal. Chem.* **1957**, *29*, 1702−1706.
(61) Zhang, X. L.; Liu, Y. F.; Zhang, X.; Hu, J. J.; Gao, M. X.; Pan, H. G. Empowering hydrogen storage performance of MgH_2 by nanoengineering and nanocatalysis. *Mater. Today Nano* **2020**, *9*, No. 100064.
(62) Ismail, M.; Juahir, N.; Mustafa, N. S. Improved hydrogen storage properties of MgH_2 co-doped with $FeCl_3$ and carbon nanotubes. *J. Phys. Chem. C* **2014**, *118*, 18878−18883.
(63) Bassetti, A.; Bonetti, E.; Pasquini, L.; Montone, A.; Grbovic, J.; Antisari, M. V. Hydrogen desorption from ball milled MgH_2 catalyzed with Fe. *Eur. Phys. J. B* **2005**, *43*, 19−27.
(64) Zhang, L.; Ji, L.; Yao, Z.; Yan, N.; Sun, Z.; Yang, X.; Zhu, X.; Hu, S.; Chen, L. Facile synthesized Fe nanosheets as superior active catalyst for hydrogen storage in MgH_2. *Int. J. Hydrogen Energy* **2019**, *44*, 21955−21964.
(65) Mao, J.; Guo, Z.; Yu, X.; Liu, H.; Wu, Z.; Ni, J. Enhanced hydrogen sorption properties of Ni and Co-catalyzed MgH_2. *Int. J. Hydrogen Energy* **2010**, *35*, 4569−4575.
(66) Huot, J.; Boily, S.; Guther, V.; Schulz, R. Synthesis of Na_3AlH_6 and Na_2LiAlH_6 by mechanical alloying. *J. Alloys Compd.* **1999**, *283*, 304−306.

https://doi.org/10.1021/acsomega.1c02208
ACS Omega 2021, 6, 18948−18956